

CRI-HOM: a novel chemical mechanism for simulating highly oxygenated organic molecules (HOMs) in global chemistry–aerosol–climate models

James Weber, Scott Archer-Nicholls, Paul Griffiths, Torsten Berndt, Michael Jenkin, Hamish Gordon, Christoph Knöte, Alexander T. Archibald

Angaben zur Veröffentlichung / Publication details:

Weber, James, Scott Archer-Nicholls, Paul Griffiths, Torsten Berndt, Michael Jenkin, Hamish Gordon, Christoph Knöte, and Alexander T. Archibald. 2020. "CRI-HOM: a novel chemical mechanism for simulating highly oxygenated organic molecules (HOMs) in global chemistry–aerosol–climate models." *Atmospheric Chemistry and Physics* 20 (18): 10889–910. <https://doi.org/10.5194/acp-20-10889-2020>.



Supplement of

CRI-HOM: A novel chemical mechanism for simulating highly oxygenated organic molecules (HOMs) in global chemistry–aerosol–climate models

James Weber et al.

Correspondence to: James Weber (jmw240@cam.ac.uk)

The copyright of individual parts of the supplement might differ from the CC BY 4.0 License.

Table S1 - Summary of RO₂-RO₂ rate coefficients

Reaction	Rate Coefficient / cm ³ molecules ⁻¹ s ⁻¹	Reference	Comments
All O3RO2 + RO2 _b = 0.5 C20d	0.97 - 3.6 × 10 ⁻¹¹ (See full reaction list)	Berndt et al., 2018b	Derived from data from Berndt et al., 2018b
All OHRO2 + RO2 _b = 0.5 C20d	0.4 - 3.5 × 10 ⁻¹¹ (See full reaction list)	Berndt et al., 2018b	Derived from data from Berndt et al., 2018b
All O3RO2 + RO2 _b = C10x/CARB16	1.68 × 10 ⁻¹²	Molteni et al., 2019	
All O3RO2 + RO2 _b = Closed shell + peroxy radical	1.68 × 10 ⁻¹²	Molteni et al., 2019 Jenkin et al., 2019a	
RN26BO2 + RO2 _m , RO2 _s = C10x/TNCARB26	8.3 × 10 ⁻¹³	Jenkin et al., 2019a*	Weighted average of rate coefficients
RTN28AO2 + RO2 _b , RO2 _m , RO2 _s = Closed shell	5.9 × 10 ⁻¹³	MCM	Weighted average of RO2 rate coefficients for species APINAO2 and APINBO2
RTN28BO2 + RO2 _m , RO2 _s = Closed shell + peroxy radical	6.70 × 10 ⁻¹⁵	MCM	MCM value for species APINCO2
2nd – 5th gen O3RO2 + RO2 _m , RO2 _s = Closed shell + peroxy radical	5 × 10 ⁻¹² – 1 × 10 ⁻¹¹ (See full reaction list)	Roldin et al., 2019	Increases with increasing O3RO2 functionality
2nd – 5th gen OHRO2 + RO2 _b , RO2 _m , RO2 _s = Closed shell + peroxy radical	5 × 10 ⁻¹² – 1 × 10 ⁻¹¹ (See full reaction list)	Roldin et al., 2019	Increases with increasing OHRO2 functionality
All O3RO2 + RO2 _m = C15d	3.9 - 7.5 × 10 ⁻¹² (See full reaction list)	Berndt et al., 2018b	Based on Berndt et al, then fitted to data

All OHRO2 + RO2 _m = C15d	$1.8 - 3.75 \times 10^{-12}$ (See full reaction list)	Berndt et al., 2018b	Based on Berndt et al, then fitted to data
---	--	----------------------	---

* The rate coefficient for the production of the closed shell and alkoxy radical from reaction of the first generation O3RO2 species, RN26BO2, with RO2_m and RO2_s was taken to be the average of the rate coefficients of the three actual species (C107O2, C109O2 and C10BO2 using the notation of Molteni et al (2019)), weighted by the branching ratio of their production. The rate coefficients for C107O2, C109O2 and C10BO2 were calculated using the methodology of Jenkin et al (2019a).

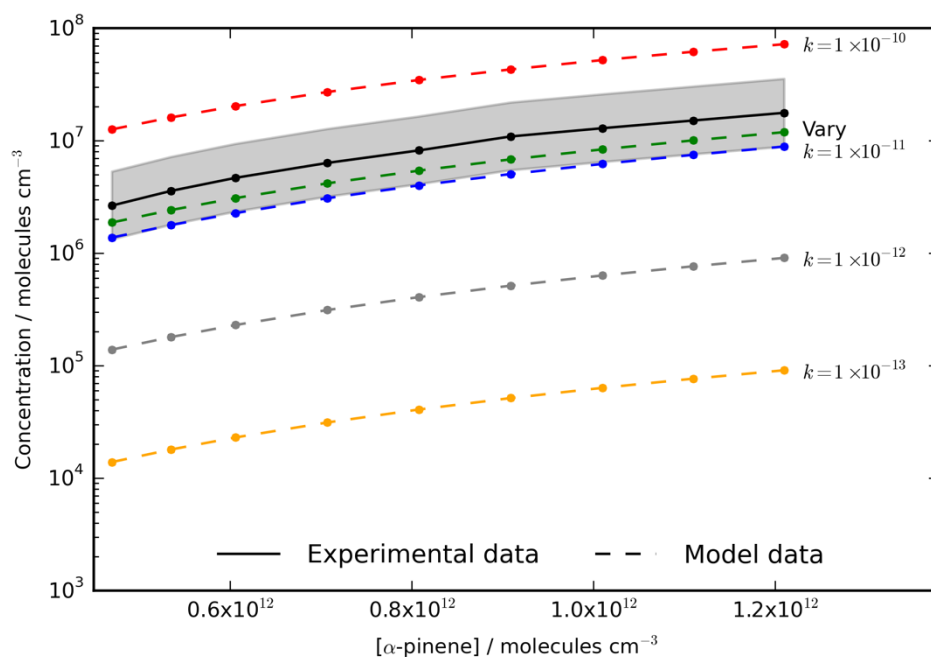


Figure S1 – Effect of C20d formation rate coefficient on model performance compared to observations from Berndt et al (2018b) under varying initial conditions of α -pinene (Simulation A, Table 3). The model was able to reproduce observed concentrations within experimental error (shaded region) here and in Fig 5 when the rate coefficients were increased with increasing peroxy radical functionalisation (line marked “Vary”). The lines with $k = 1 \times 10^{-10}$, 1×10^{-11} , 1×10^{-12} and 1×10^{-13} show model performance when the specified rate coefficient (in units of $\text{cm}^3 \text{ molecules}^{-1} \text{ s}^{-1}$) was used for all O3RO2 and OHRO2. The simulations with accretion formation rate coefficients suggested by Roldin et al (2019) ($\sim 10^{-13}$ - $10^{-12} \text{ cm}^3 \text{ molecules}^{-1} \text{ s}^{-1}$) produced significantly lower C20d concentrations while using rate coefficients suggested by Molteni et al (2019) ($\geq 10^{-10} \text{ cm}^3 \text{ molecules}^{-1} \text{ s}^{-1}$) overpredicted C20d concentrations.

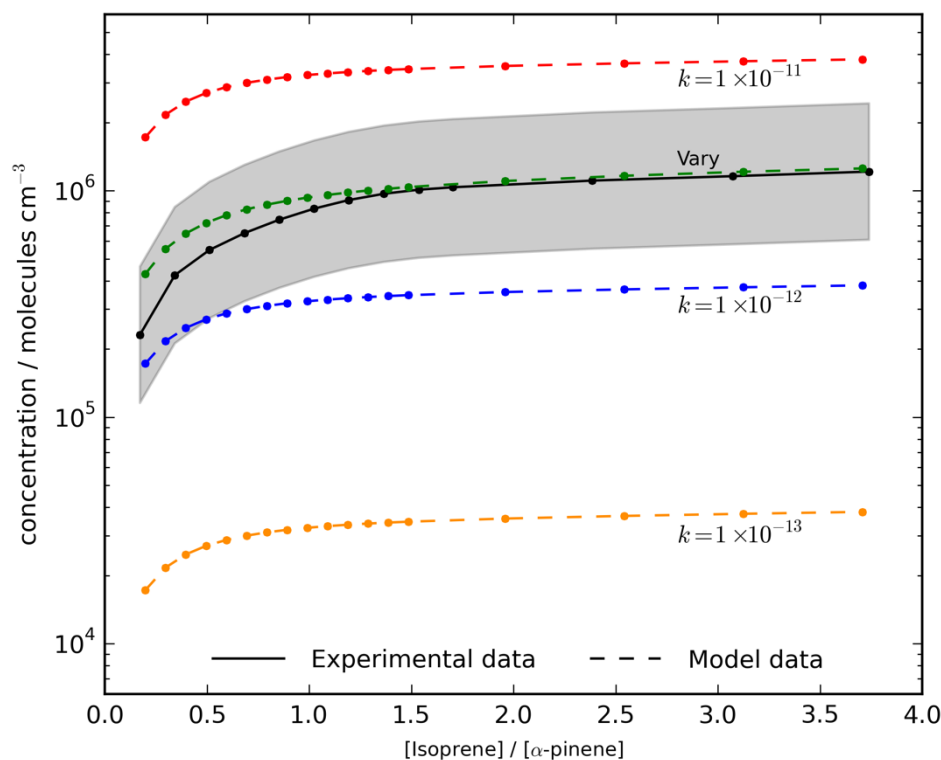


Figure S2 – Effect of C15d formation rate coefficient on model performance compared to observations from Berndt et al (2018b) under conditions of fixed initial α -pinene concentration and varying initial isoprene concentration (Simulation B, Table 3). The model was able to replicate the general trend of increasing C15d with isoprene when the rate coefficients were increased with increasing peroxy radical functionalisation (line marked “Vary”), reproducing observation within experimental error (shaded region). The lines with $k=1\times10^{-11}$, 1×10^{-12} and 1×10^{-13} show model performance when the specified rate coefficient (in units of $\text{cm}^3 \text{molecules}^{-1} \text{s}^{-1}$) was used for all O3RO2 and OHRO2.

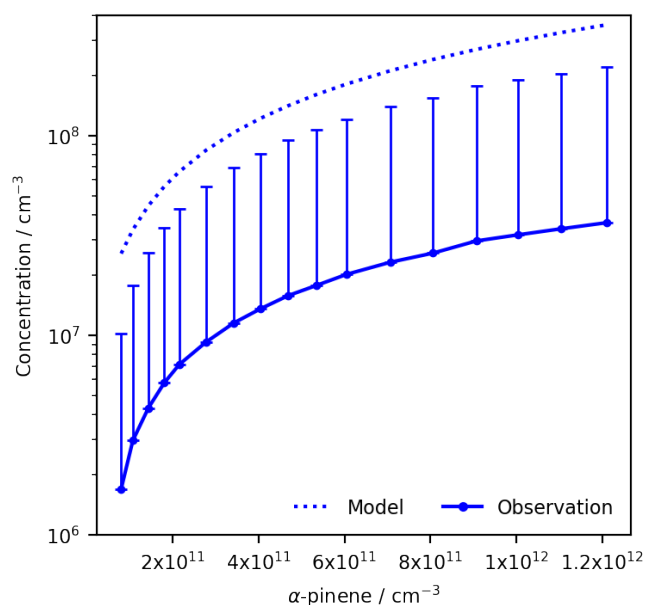


Figure S3 – 1st generation OHRO2 observation (Berndt et al., 2018b) and modelled with estimated experimental underprediction of factor of 5. Reasons for observation-model discrepancy are discussed in the main text.

Table S2 - Summary of HOM mechanisms and autoxidation activation energies

Mechanism	Autoxidation Activation Energy / K	Comments
-----------	------------------------------------	----------

HOM _{TI}	N/A - temperature independent	Autoxidation coefficients based on fitting from data from Berndt et al (2018b) at 297K
HOM ₆₀₀₀	6000	Representing possible lower bound of activation energy
HOM ₉₀₀₀	9000	Representing possible middle value of activation energy
HOM ₁₂₀₇₇	12077	Value suggested by Roldin et al (2019)

30

HOM Yield Equations

The yields for 10-carbon HOMs from ozonolysis (γ_{C10z}), OH oxidation (γ_{C10x}) and the total HOM yield (γ_{total}) are given by Eq. 1, Eq. 2 and Eq. 3 respectively.

35
$$\gamma_{C10x} = \frac{[C10x](k_{OH+HOM}+CS+J)}{k_{OH}[OH][AP]} \quad (1)$$

$$\gamma_{C10z} = \frac{[C10z](k_{OH+HOM}+CS+J)}{k_{O_3}[O_3][AP]} \quad (2)$$

40
$$\gamma_{total} = \frac{([C10z]+[C10x])(k_{OH+HOM}+CS+J)}{(k_{O_3}[O_3]+k_{OH}[OH])[AP]} \quad (3)$$

where $[O_3]$, $[OH]$, $[C10z]$ and $[C10x]$ are the concentrations of O_3 , OH and the 10-carbon HOMs formed from ozonolysis and OH oxidation respectively, k_{OH+HOM} is the rate coefficient for the reactions of HOMs with OH, CS is the HOM condensation sink, J is the HOM photolysis frequency and k_{O_3} and k_{OH} are the reaction rate coefficients of α -pinene with O_3 and OH respectively.

45

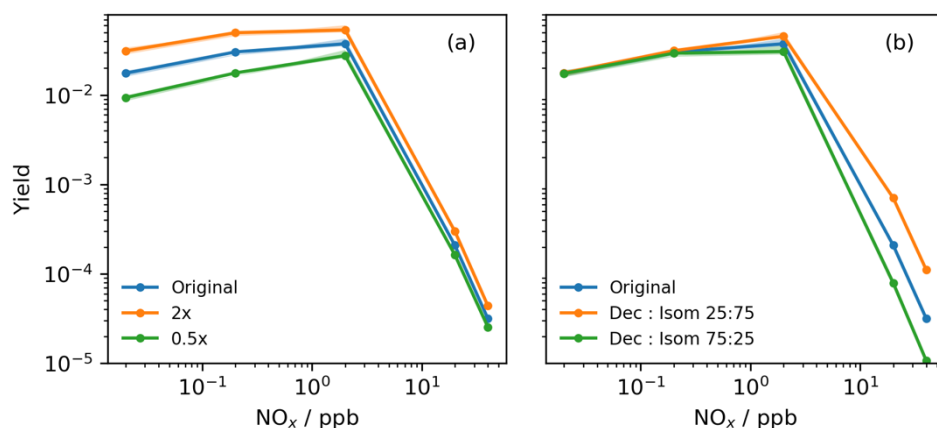


Figure S4 – Modelled HOM yield at 290 K showing with (a) scaling of k14, k15 rate coefficients and (b) perturbations of the alkoxy decomposition-isomerisation branching ratio (originally 50:50).

50

Comparison to CRI v2.2

The new mechanism and the CRI v2.2 were run in a box model (Simulation D, Table 3) for 8 days with varying temperature (298 K average, amplitude of 4 K) and emissions of isoprene and α -pinene varying sinusoidally (Fig S3). Time-independent base NO emissions of 4.7×10^9 molecules $\text{m}^{-2} \text{s}^{-1}$ were used with scaling factors of 1, 3, 10, 30, 100 and 200 employed in a manner consistent with Jenkin et al (2015). Time dependent isoprene emissions reached a maximum of 1.1×10^{12} molecules $\text{m}^{-2} \text{s}^{-1}$ at 13:00 local time and had an average of 7.1×10^{11} molecules $\text{m}^{-2} \text{s}^{-1}$ over the period 06:00 to 18:00, similar to emissions used in Jenkin et al (2015) and Bates et al (2019). Time dependent base α -pinene emissions with a mean of 3.23×10^9 molecules $\text{m}^{-2} \text{s}^{-1}$ and maximum of 5.30×10^9 molecules $\text{m}^{-2} \text{s}^{-1}$ at 1500 hours were applied. Further runs were performed with α -pinene emissions scaled by factors of 10^{-3} , 10^{-2} , 0.1, 0.2, 0.5, 1, 2, 3 and 5 to investigate the model's performance. Initial conditions of CH_4 (1.8 ppm), CO (100 ppb), O_3 (20 ppb) and HCHO (300 ppt) were applied.

Photolysis frequencies simulating conditions at the equator also varied in the diurnal cycle. The box model simulated an instantaneously well-mixed planetary boundary with mixing with the free troposphere (with same composition of initial conditions) represented by the box height increasing from 250 m at night to 1500 m at midday before collapsing back to 250 m at 2100 hours.

The "concentration" of a species was taken to be the mean daytime concentration on the 8th day, the metric used by Jenkin et al (2015) and Bates et al (2019). The performance of all the HOM mechanisms (HOM_{TL}, HOM₆₀₀₀, HOM₉₀₀₀ and HOM₁₂₀₇₇) was compared to the CRI v2.2.

The HOM mechanisms matched the CRI extremely well for OH, O_3 , NO, NO_2 , HO_2 , α -pinene and isoprene as well as the hydroperoxides and nitrates derived from isoprene, methyl vinyl ketone and methacrolein, and the important SOA precursor isoprene epoxy diol (IEPOX)).

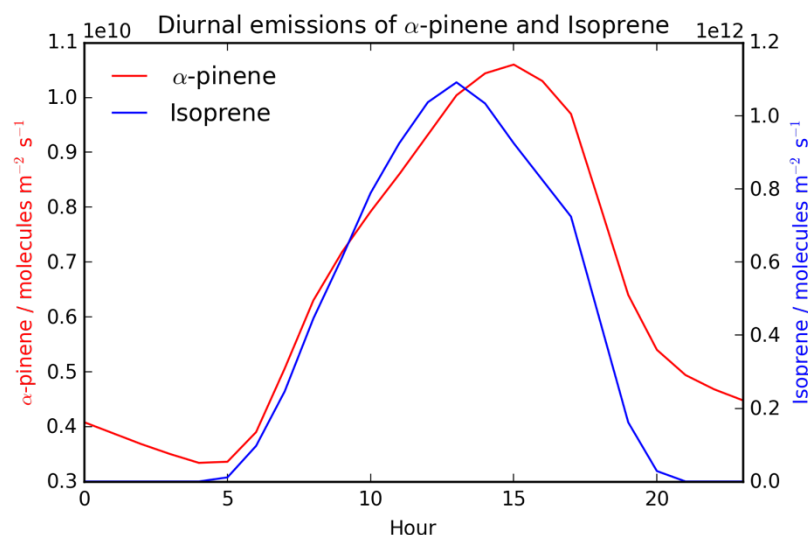
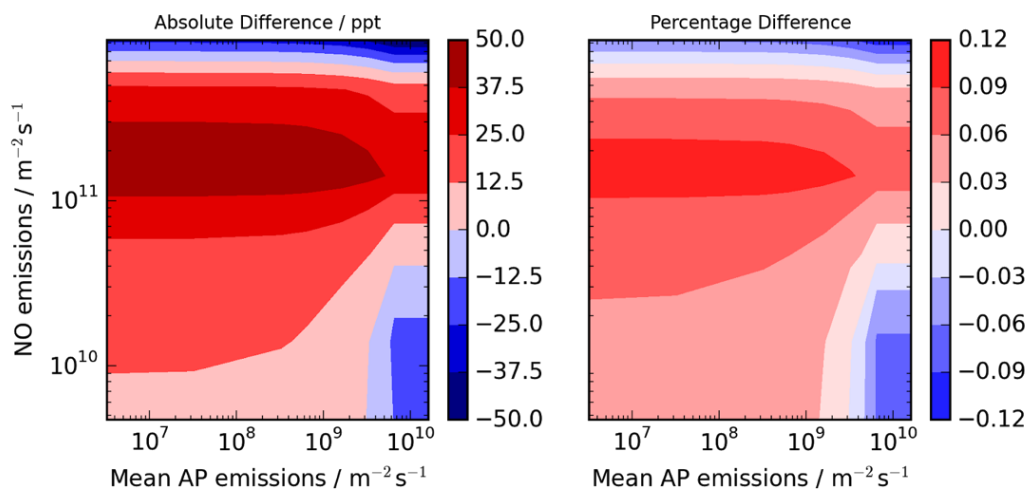
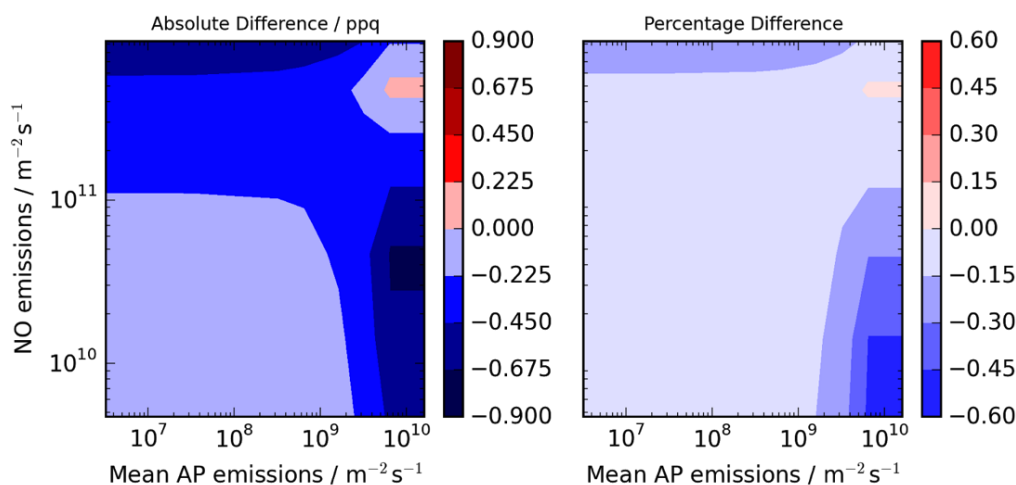


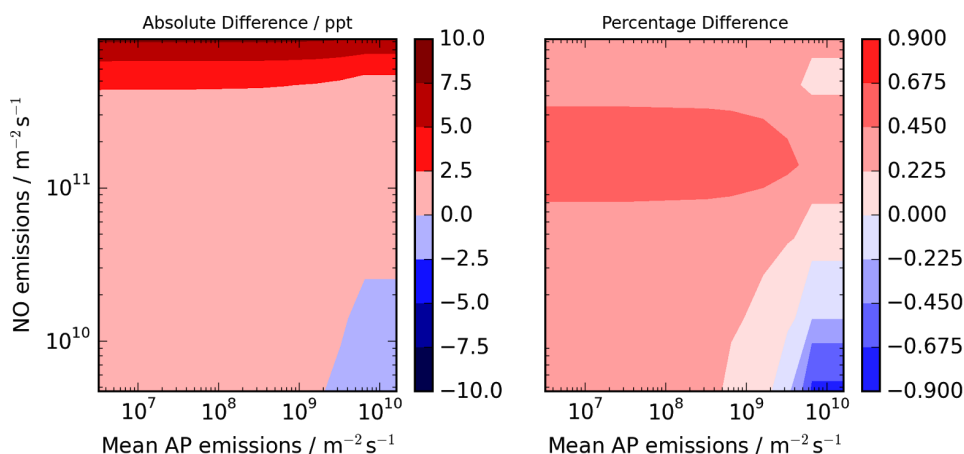
Figure S5 - Diurnal cycle of emissions of α -pinene and isoprene for 8-day comparison of CRI v2.2 R5 with HOM mechanism versions.



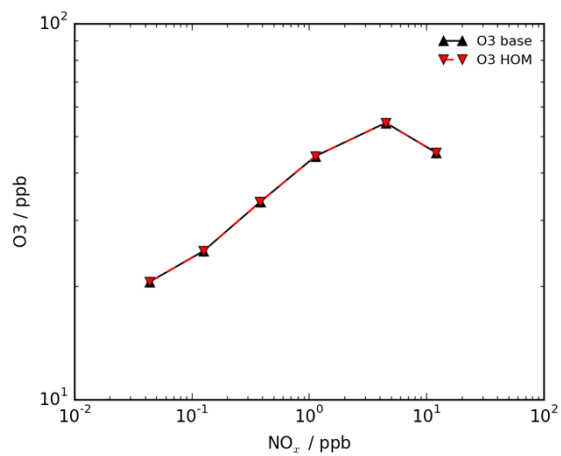
80 **Figure S6 - Absolute and percentage difference in 8th day daylight mean O₃ between the CRI v2.2 R5 and the HOM₉₀₀₀ mechanism. The difference between mechanisms is less than ± 0.05 ppb.**



85 **Figure S7 - Absolute and percentage difference in 8th day daylight mean OH between the CRI v2.2 R5 and the HOM₉₀₀₀ mechanism. The difference between mechanisms is less than $\pm 0.3\%$ for the vast majority of the emissions space with the difference exceeding this only under very high emissions of α -pinene.**



90 **Figure S8 - Absolute difference in 8th day daylight mean NO between the CRI v2.2 R5 and the HOM₉₀₀₀ mechanism. The difference between mechanisms is less than ± 2.5 ppt for the vast majority of the emissions space with the difference exceeding this only under very high emissions of NO and α -pinene.**



95 **Figure S9 - 8th day daylight mean O₃ in CRI v2.2 R5 and HOM₉₀₀₀ model**

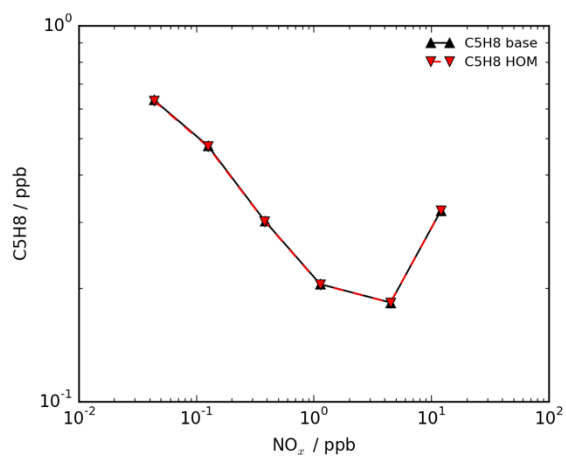


Figure S10 - 8th day daylight mean isoprene in CRI v2.2 R5 and HOM₉₀₀₀ model

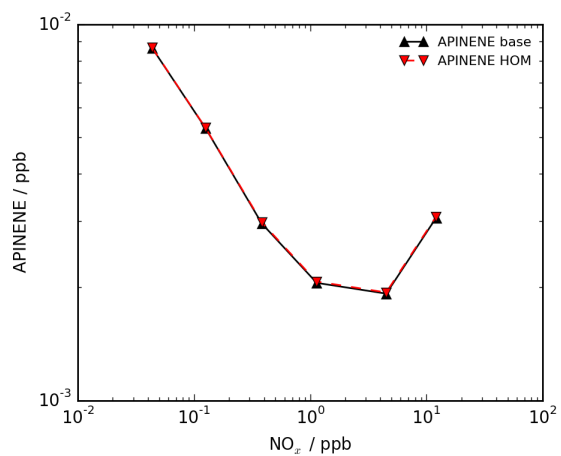


Figure S11 - 8th day daylight mean α -pinene in CRI v2.2 R5 and HOM₉₀₀₀ model

100

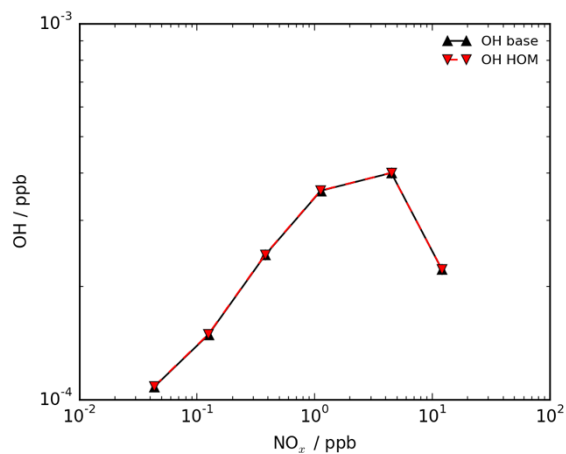


Figure S12 - 8th day daylight mean OH in CRI v2.2 R5 and HOM₉₀₀₀ model

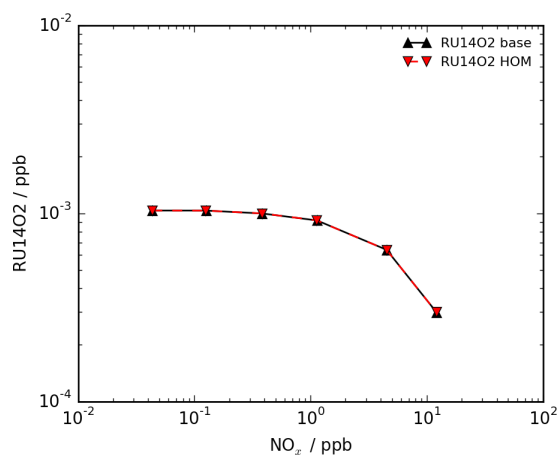


Figure S13 - 8th day daylight mean 1st generation isoprene peroxy radical in CRI v2.2 R5 and HOM₉₀₀₀ model

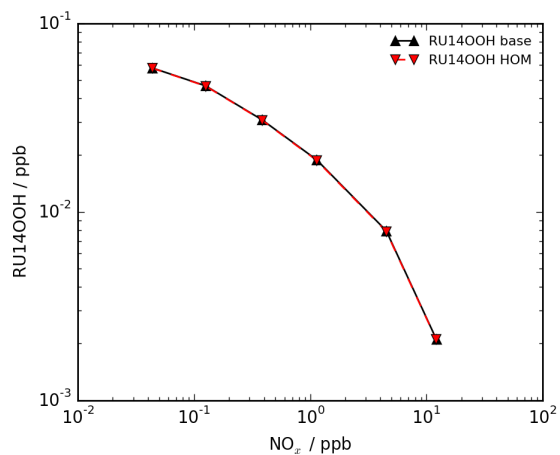


Figure S14 - 8th day daylight mean 1st generation isoprene hydroperoxide in CRI v2.2 R5 and HOM₉₀₀₀ model

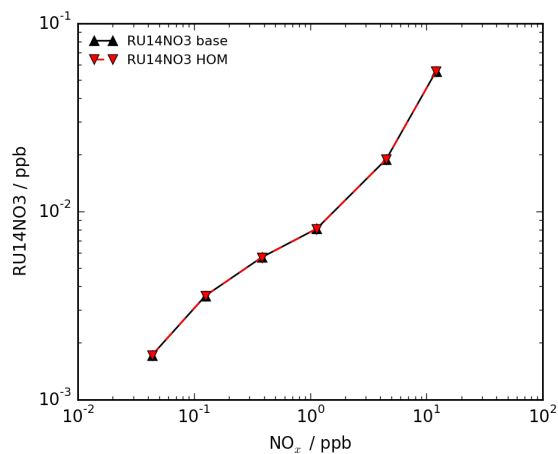


Figure S15 - 8th day daylight mean 1st generation isoprene nitrate in CRI v2.2 R5 and HOM₉₀₀₀ model

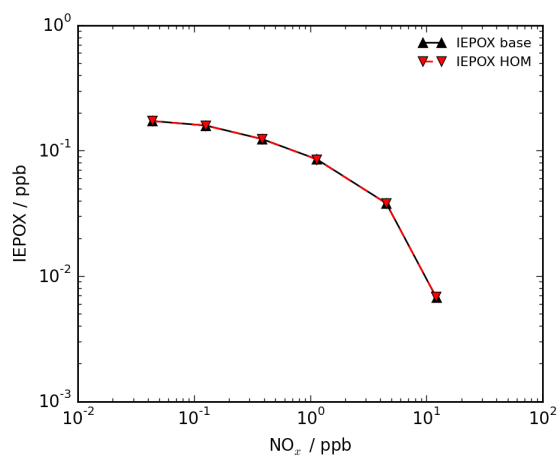


Figure S16 - 8th day daylight mean isoprene epoxydiol in CRI v2.2 R5 and HOM₉₀₀₀ model

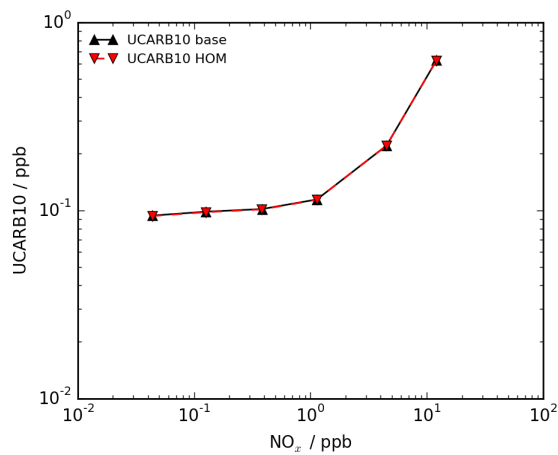


Figure S17 - 8th day daylight mean combined methyl vinyl ketone and methacrolein in CRI v2.2 R5 and HOM₉₀₀₀ model

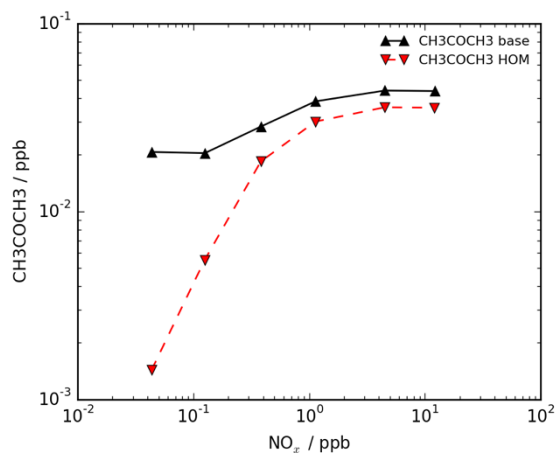


Figure S18 - 8th day daylight mean combined acetone in CRI v2.2 R5 and HOM₉₀₀₀ model. The difference was attributed to the added competition supplied by the autoxidation pathways, diverting the degradation of α -pinene away from the traditional pathways which form acetone. However, this discrepancy between mechanisms did not led to significant disagreement between the HOM mechanism and CRI v2.2 R5 for O₃ and OH concentrations.

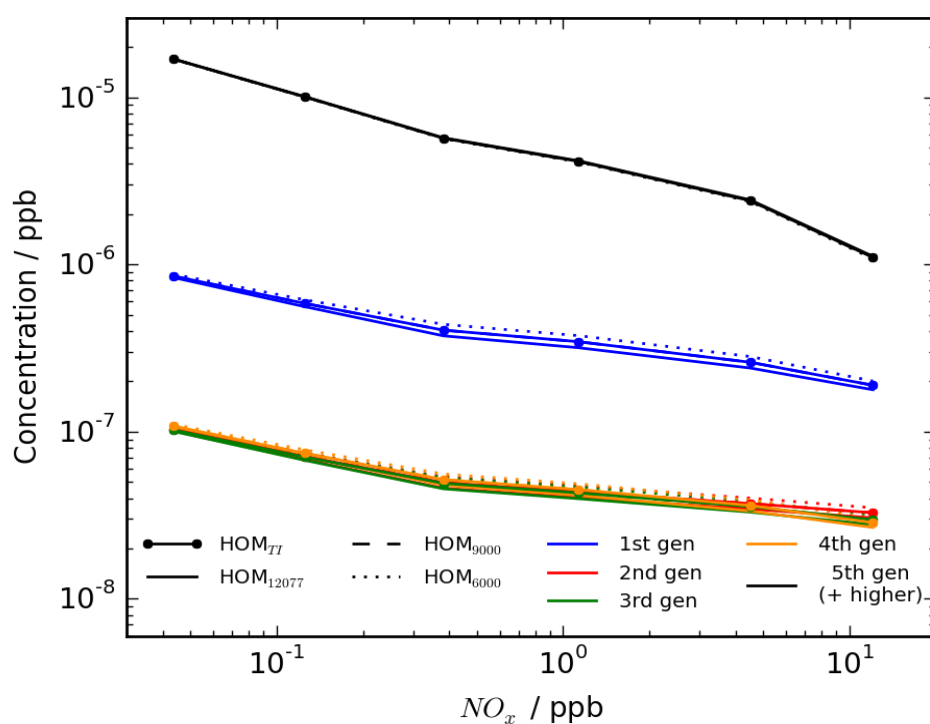


Figure S19 – Peroxy radicals from ozonolysis (O3RO2) exhibiting a decrease with NO_x and the clear dominance of the highest generation peroxy radical. Negligible difference is observed between the 4 HOM mechanisms for each peroxy radical.

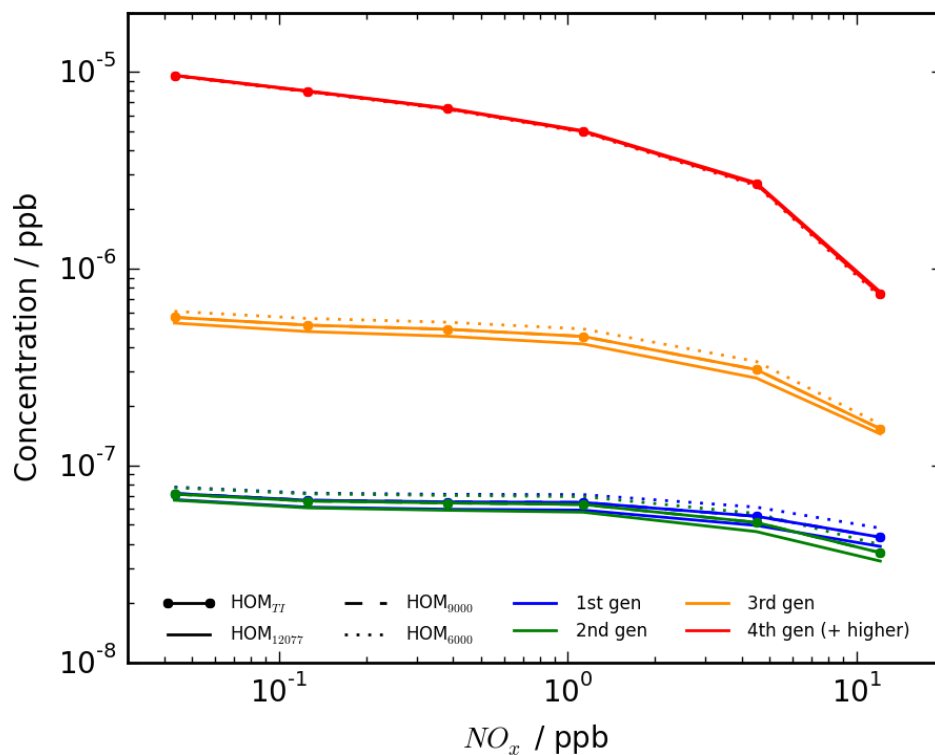


Figure S20 – Peroxy radicals from OH oxidation (OHRO2) exhibiting a decrease with NO_x and the clear dominance of the highest generation peroxy radical. Negligible difference is observed between the 4 HOM mechanisms for each peroxy radical.

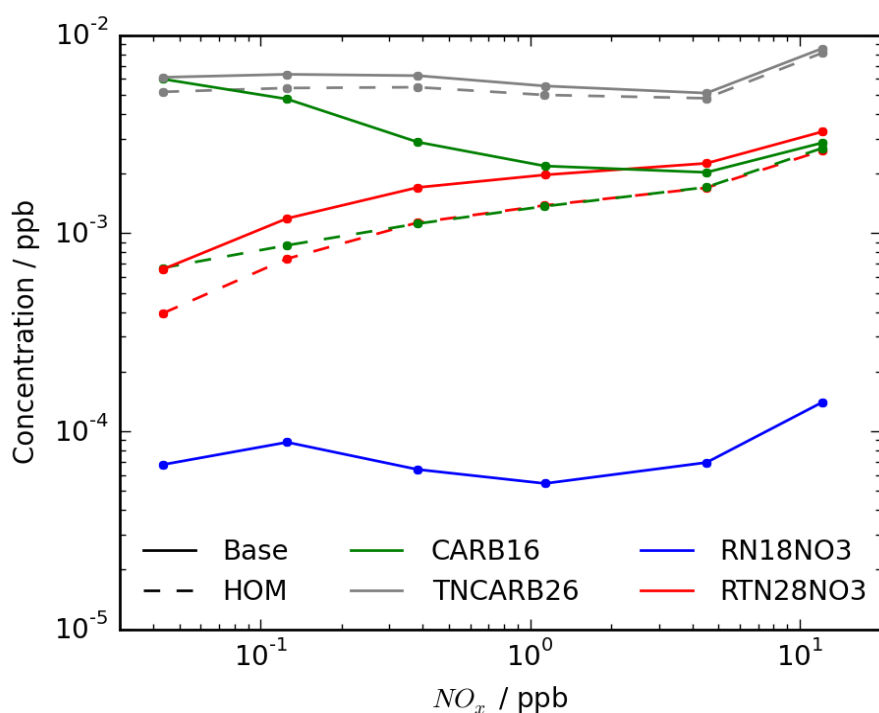
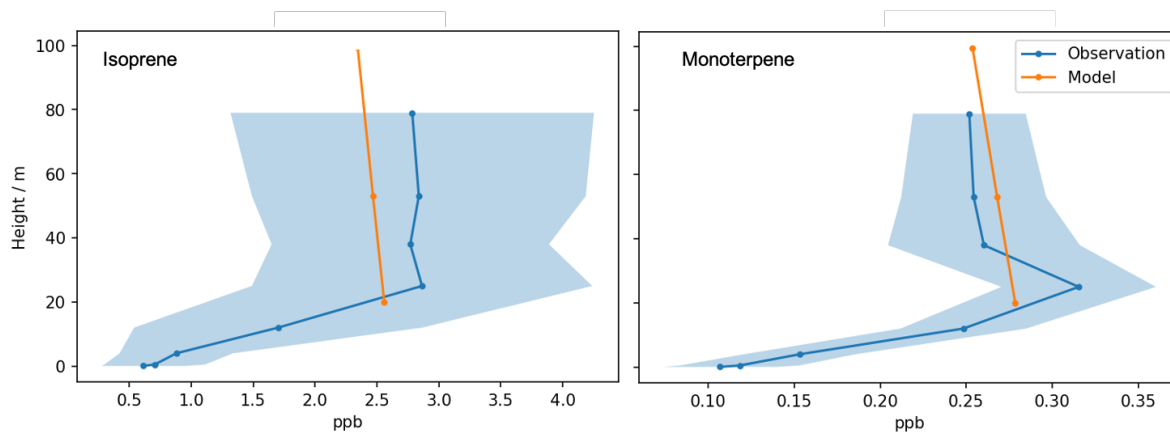
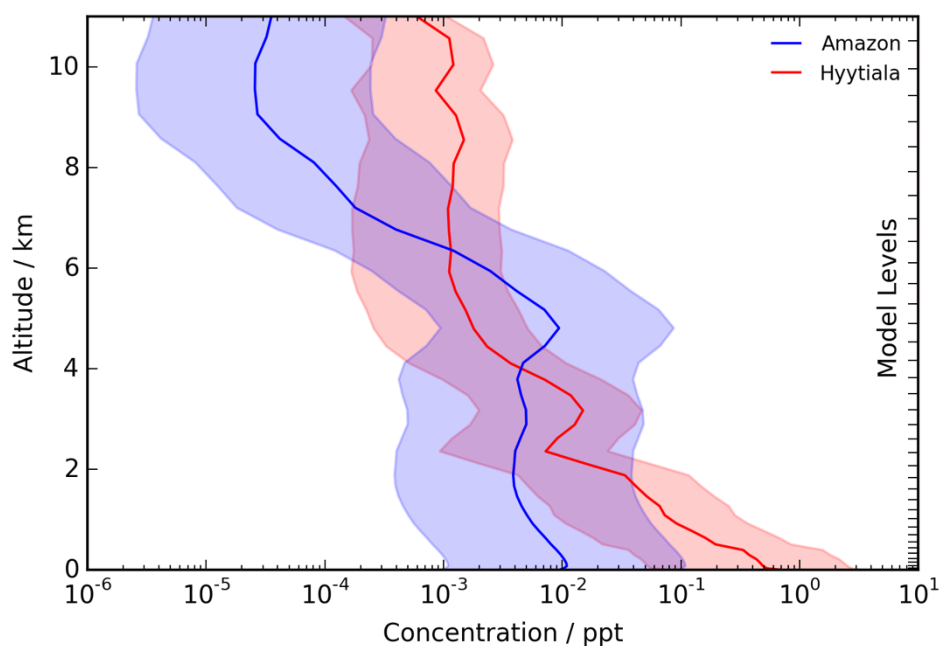


Figure S21 – Closed shell species in base mechanism compared to HOM_{TI} mechanism. The lower concentrations of TNCARB26, CARB16 and RTN28NO3 were attributed to the increased competition from the autoxidation pathways in the HOM mechanism. RN18NO3 was significantly lower in the HOM mechanisms (not shown) as discussed in the main text.



140 **Figure S22 – Observed concentrations of isoprene (left) and monoterpene (right) at the ATTO tower at 1:30-2:30 pm in June 2013 (Yáñez-Serrano et al., 2015) (shading shows standard deviation of observational data) and modelled concentrations of species.**



145 **Figure S23 – Total HOM concentrations in Amazon and Hyytiälä with shaded region showing the effect of increasing/decreasing CS by a factor of 10. The value of the CS has a significant influence on HOM concentrations.**

Table S3 – Species and physical parameters used in the HOM altitude profile modelling. Note that for nucleation calculations, the same input species and parameters were used but all data were monthly means.

Data from UKCA run (2pm 16th June, averaged over 2010-2104)	Data from UKESM Historical
Temperature, pressure, O ₃ , OH, isoprene, monoterpene*, NO, NO ₂ , NO ₃ , N ₂ O ₅ , CO, HO ₂ , H ₂ O	CH ₄ , CO, HCHO, CH ₃ O ₂ , C ₂ H ₅ O ₂ , isoprene nitrate and hydroperoxides, H ₂ O ₂ , CH ₃ OOH, HONO, C ₂ H ₆ , C ₂ H ₅ OOH, CH ₃ CHO, PAN, C ₃ H ₈ , C ₃ H ₇ OOH, C ₂ H ₅ CHO, CH ₃ NO ₃ , Methacrolein, Methylglyoxal, HCOOH, CH ₃ CO ₃ , C ₃ H ₇ O ₂ , C ₂ H ₅ CO ₃ , CH ₃ OH

* The modelled monoterpene concentration was halved to approximate the α -pinene concentration (Rinne et al., 2002)

150 **Table S4 - Values of surface level CS and local time of run used for HOM altitude profiles (Lee et al., 2016)**

	Location		
	Hyttiala	Manaus	Brent, Alabama
CS / s ⁻¹	0.004	0.9	0.012 ± 0.006
Local time	14:00	14:00	12:00

Nucleation Parameterisations

The rates of neutral and ion-induced pure biogenic nucleation (J_n and J_{iin} respectively) are described by the parameterisations (Kirkby et al (2016)) in Eq. 4 and Eq. 5:

$$J_n = a_1[HOM]^{a_2 + \frac{a_5}{[HOM]}} \quad (4)$$

$$J_{iin} = a_3[HOM]^{a_4 + \frac{a_5}{[HOM]}}[n_{\pm}] \quad (5)$$

Where a_i are fitted parameters and $[n_{\pm}]$ the concentration of ions calculated by method described Kirkby et al (2016). In this work, no distinction was made between the different HOM species; the $[HOM]$ term was taken as the sum of all HOM species. In reality, the larger accretion products are likely to be better at nucleating due to their lower volatility and even among 10-carbon HOMs, more oxidised species will also be more proficient at new particle formation. The condensation sink for ions was calculated by summing over aerosol modes and (Eq. 6).

$$CS = \frac{2kT\mu}{\varepsilon} \sum (wd \times c) \times 10^6 \quad (6)$$

Where k is the Boltzmann constant, T temperature (in Kelvin), $\mu = 1.2 \times 10^{-4} \text{ m}^2 \text{ V}^{-1} \text{ s}^{-1}$, $\varepsilon = 1.6022 \times 10^{-19} \text{ C}$, wd is the wet diameter (in m) of the aerosol mode and c the mode's particle concentration (per cm³) (wd and c were taken from UKCA run).

The ion loss rate, X , was then calculated as the sum of the condensation and nucleation sinks (Eq. 7).

$$X = CS + a_3[HOM]^{a_4 + \frac{a_5}{[HOM]}} \quad (7)$$

The recombination coefficient, α , is given by Eq. 8:

$$\alpha = 6 \times 10^{-8} \sqrt{\frac{300}{T}} + 6 \times 10^{-26} c_{air} \left(\frac{300}{T}\right)^4 \quad (8)$$

Where c_{air} is the concentration of air in molecules per cm³.

$$[n_{\pm}] = \frac{\sqrt{(X^2 - 4\alpha q)} - X}{2\alpha} \quad (9)$$

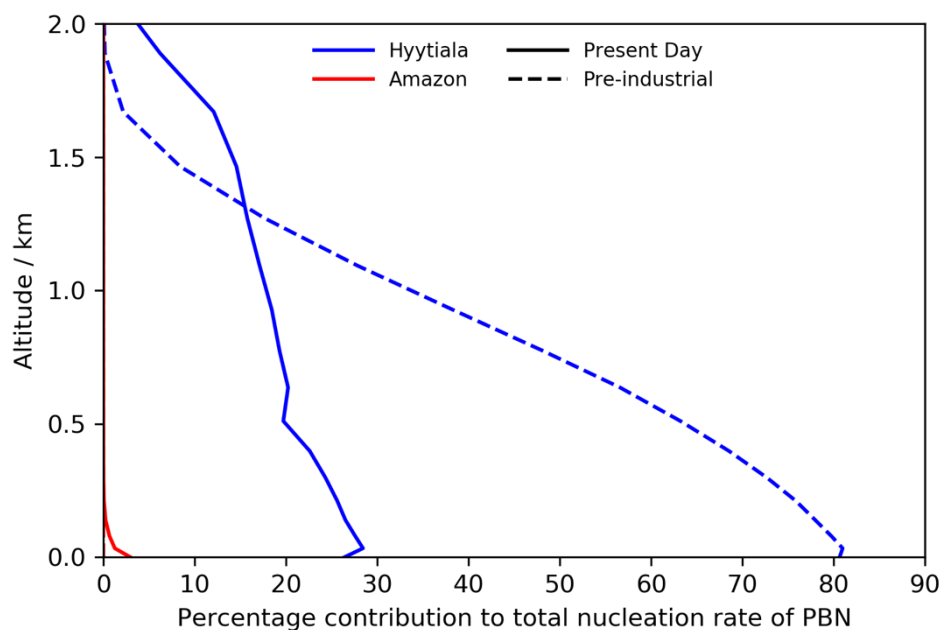
Where q is the rate of ion-pair production in cm⁻³ s⁻¹.

The sulphuric acid activation parameterisation used was that developed by Kulmala et al (2006) with coefficient from Sihto et al (2006) as used by Scott et al (2014) (Eq. 10).

$$J_{act} = A[H_2SO_4]$$

(10)

Where $A=2 \times 10^{-6} \text{ s}^{-1}$



180 **Figure S24 – Percentage contribution to total nucleation rate (PBN + SA_{act}) of PBN. Significant increase is predicted for the PI Hyytiala case in particular, indicating the important implications of including PBN in climate models.**

Changes to CRI v2.2 R5 mechanism

Simple rate coefficients (e.g. k_{RO_2NO}) and photolysis frequencies (e.g. J_{41}) were taken from CRI (Jenkin et al., 2008, Jenkin
 185 et al., 2019b). Unless otherwise stated, unimolecular rate coefficients have units of s^{-1} . The peroxy radical pools (RO_{2b} , RO_{2m} , RO_{2s} and RO_2) represent the total concentration of peroxy radicals falling within the respective pool. In the mechanism used
 in modelling, certain reactions were lumped together with product fractions weighted by relative rate coefficients to reduce
 the total number of reactions. For clarity, reactions have been decomposed below. The autoxidation coefficients provided are
 those fitted at 297 K. Table S5 shows the expressions for the autoxidation coefficients in the 3 temperature dependent
 190 mechanisms.

The standard reactions rate coefficients used by the CRI are as follows:

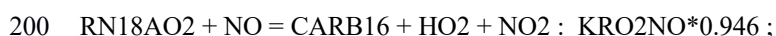
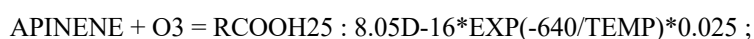
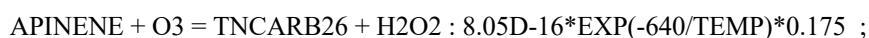
$$KRO_2NO = 2.7D-12 * EXP(390/TEMP)$$

$$KRO_2HO_2 = 2.91D-13 * EXP(1300/TEMP)$$

$$KRO_2NO_3 = 2.3D-12$$

195 Reactions removed from CRI v2.2 R5 mechanism

Ozonolysis of alpha pinene and treatment of resulting peroxy radical RN18AO2



$\text{RN18AO2} + \text{NO} = \text{RN18NO3} : \text{KRO2NO} * 0.054 ;$

$\text{RN18AO2} + \text{NO3} = \text{CARB16} + \text{HO2} + \text{NO2} : \text{KRO2NO3} ;$

$\text{RN18AO2} + \text{HO2} = \text{RN18OOH} : \text{KRO2HO2} * 0.770 ;$

$\text{RN18AO2} = \text{CARB16} + \text{HO2} : 8.80\text{D-13} * \text{RO2} ;$

205 **OH oxidation of alpha pinene and treatment of resulting peroxy radical RTN28O2**

$\text{APINENE} + \text{OH} = \text{RTN28O2} : 1.20\text{D-11} * \text{EXP}(444/\text{TEMP}) ;$

$\text{RTN28O2} + \text{NO} = \text{TNCARB26} + \text{HO2} + \text{NO2} : \text{KRO2NO} * 0.767 * 0.915 ;$

$\text{RTN28O2} + \text{NO} = \text{CH3COCH3} + \text{RN19O2} + \text{NO2} : \text{KRO2NO} * 0.767 * 0.085 ;$

$\text{RTN28O2} + \text{NO} = \text{RTN28NO3} : \text{KRO2NO} * 0.233 ;$

210 **RTN28O2 + NO3 = TNCARB26 + HO2 + NO2 : KRO2NO3 ;**

$\text{RTN28O2} + \text{HO2} = \text{RTN28OOH} : \text{KRO2HO2} * 0.914 ;$

$\text{RTN28O2} = \text{TNCARB26} + \text{HO2} : 2.85\text{D-13} * \text{RO2} ;$

Reactions added

215 **Ozonolysis of α -pinene producing 1st generation O3RO2, RN26BO2 - branching ratio set to 50% based on experimental observations of Berndt et al (2018b)**

1. $\text{APINENE} + \text{O3} = 0.175\text{TNCARB26} + 0.025\text{RCOOH25} + 0.8\text{OH} + 0.5\text{RN26BO2} + 0.3\text{RTN24O2} : 8.05\text{E-16} * \text{EXP}(-640/\text{TEMP}) ;$

Reactions of RN26BO2

Reaction with HO2 forms hydroperoxide species already in CRI, not a HOM due to insufficient oxygens.

220 **2. $\text{RN26BO2} + \text{HO2} = \text{RTN26OOH} : \text{KRO2HO2} * 0.9 ;$**

Reaction with NO, NO₃ forms next generation O3RO2 via alkoxy radical isomerisation and fragmentation products (smaller RO2, RN9O2, and closed shell species, CARB16) at 50:50 branching ratio). NO also forms small yield of RN18NO3, estimated from original CRI v2.2 R5.

3. $\text{RN26BO2} + \text{NO} = 0.025\text{RTN28NO3} + 0.487\text{RN25BO2O2} + 0.487\text{CARB16} + 0.487\text{RN9O2} + 0.975\text{NO2} : \text{KRO2NO} ;$

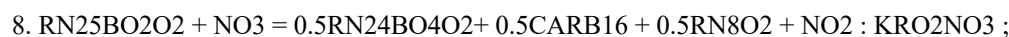
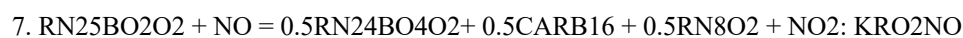
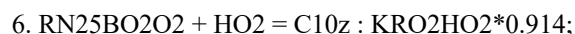
225 **4. $\text{RN26BO2} + \text{NO3} = 0.5\text{RN25BO2O2} + 0.5\text{CARB16} + 0.5\text{RN9O2} + \text{NO2} : \text{KRO2NO3} ;$**

Autoxidation of RN26BO2 to 2nd generation O3RO2, RN25BO2O2

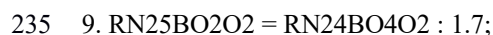
5. $\text{RN26BO2} = \text{RN25BO2O2} : 0.206 ;$

Reactions of RN25BO2O2

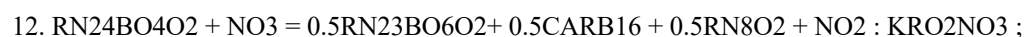
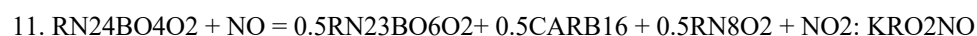
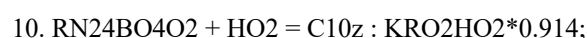
230 **Reaction with HO2 forms HOM monomer C10z as product has sufficient oxygens. Reaction with NO, NO₃ follows the same principle as RN26BO2.**



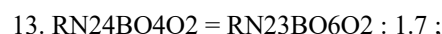
Autoxidation of RN25BO2O2 to 3rd generation O3RO2, RN24BO4O2



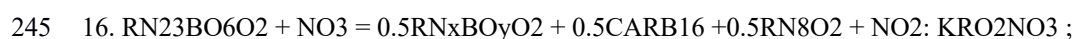
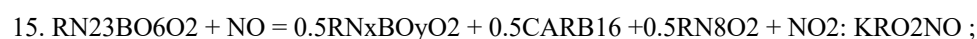
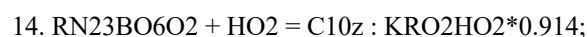
Reactions of RN24BO4O2



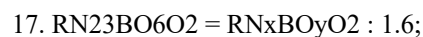
240 **Autoxidation of RN24BO4O2 to 4th generation O3RO2, RN23BO6O2**



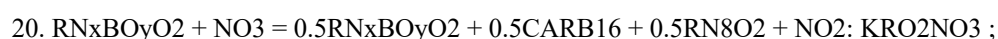
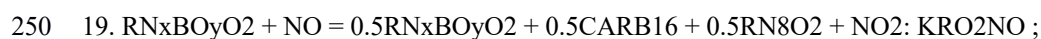
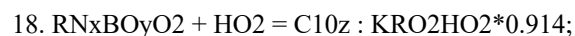
Reactions of RN23BO6O2



Autoxidation of RN23BO6O2 to lumped “5th generation and higher” O3RO2, RNxBOyO2



Reactions of RNxBOyO2 - no further autoxidation



Reactions of O3RO2 with big peroxy radical pool (RO2_b)

All reactions with RO_{2b} produce a 20-carbon accretion product at a rate coefficient from fitting to experimental data (Berndt et al., 2018b). Reactions also produce, with equal rate coefficients (from Molteni et al., 2019), closed shell species which are classified as HOMs for all cases (except for the reaction of RN26BO2 which is not sufficiently oxidised) and alkoxy radicals which go on to react as previously described in this work.

21. $\text{RN26BO2} = 0.5 \text{ C20d} : 0.97\text{E-11 RO}_{2b}$;
22. $\text{RN26BO2} = 0.5\text{TNCARB26} + 0.25\text{RN25BO2O2} + 0.25\text{CARB16} + 0.25\text{RN8O2} : 3.36\text{E-12*RO}_{2b}$;
23. $\text{RN25BO2O2} = 0.5 \text{ C20d} : 2.5\text{E-11 RO}_{2b}$;
24. $\text{RN25BO2O2} = 0.5\text{C10z} + 0.25\text{RN24BO4O2} + 0.25\text{CARB16} + 0.25\text{RN8O2} : 3.36\text{E-12*RO}_{2b}$;
25. $\text{RN24BO4O2} = 0.5 \text{ C20d} : 3.4\text{E-11 RO}_{2b}$;
26. $\text{RN24BO4O2} = \text{C10z} + 0.5 \text{ RN23BO6O2} + 0.5 \text{ CARB16} + 0.5 \text{ RN8O2} : 1.68\text{E-12 RO}_{2b}$;
26. $\text{RN24BO4O2} = 0.5\text{C10z} + 0.25\text{RN23BO6O2} + 0.25\text{CARB16} + 0.25\text{RN8O2} : 3.36\text{E-12*RO}_{2b}$;
27. $\text{RN23BO6O2} = 0.5 \text{ C20d} : 3.6\text{E-11 RO}_{2b}$;
28. $\text{RN23BO6O2} = 0.5\text{C10z} + 0.25\text{RNxB0yO2} + 0.25\text{CARB16} + 0.25\text{RN8O2} : 3.36\text{E-12*RO}_{2b}$;
29. $\text{RNxB0yO2} = 0.5 \text{ C20d} : 3.6\text{E-11 RO}_{2b}$;
30. $\text{RNxB0yO2} = 0.5\text{C10z} + 0.25\text{RNxB0yO2} + 0.25\text{CARB16} + 0.25\text{RN8O2} : 3.36\text{E-12*RO}_{2b}$;

Reactions of O₃RO₂ with medium and small peroxy radical pools (RO_{2m} and RO_{2s})

Reaction of RN26BO2 is based on corresponding species in MCM.

31. $\text{RN26BO2} = 0.5\text{RN25BO2O2} + 0.5\text{CARB16} + 0.5\text{RN9O2} : 8.13\text{E-13 (RO}_{2s}+\text{RO}_{2m})$;
- Rate coefficient and branching ratios of later generation O₃RO₂ with medium and small peroxy radical pools taken from Roldin et al (2019). The alkoxy radical produced goes on to react as described earlier in this work.
32. $\text{RN25BO2O2} = 0.3\text{RN24BO4O2} + 0.3\text{CARB16} + 0.3\text{RN8O2} + 0.4\text{C10z} : 5\text{E-12 (RO}_{2s}+\text{RO}_{2m})$;
33. $\text{RN24BO4O2} = 0.2\text{RN23BO6O2} + 0.2\text{CARB16} + 0.2\text{RN8O2} + 0.6\text{C10z} : 7\text{E-12 (RO}_{2s}+\text{RO}_{2m})$;
34. $\text{RN23BO6O2} = 0.1\text{RNxB0yO2} + 0.1\text{CARB16} + 0.1\text{RN8O2} + 0.8\text{C10z} : 9\text{E-12 (RO}_{2s}+\text{RO}_{2m})$;
35. $\text{RNxB0yO2} = 0.1\text{RNxB0yO2} + 0.1\text{CARB16} + 0.1\text{RN8O2} + 0.8\text{C10z} : 1\text{E-11 (RO}_{2s}+\text{RO}_{2m})$;

Rate coefficient of O3RO2 with isoprene-derived peroxy radical from fitting of model to experimental data (Berndt et al, 2018b).

36. $RN26BO2 = 0.667C15d : 3.9E-12 RO2_m ;$

285 37. $RN25BO2O2 = 0.667C15d : 5.2E-12 RO2_m ;$

38. $RN24BO4O2 = 0.667C15d : 6.5E-12 RO2_m ;$

39. $RN23BO6O2 = 0.667C15d : 6.5E-12 RO2_m ;$

40. $RN_xBO_yO2 = 0.667C15d : 7.5E-12 RO2_m ;$

OH oxidation of alpha pinene producing two OHRO2 - RTN28AO2 + RTN28BO2

290 41. $APINENE + OH = 0.78 RTN28AO2 + 0.22 RTN28BO2 : 1.20E-11 * EXP(440/TEMP);$

Reactions of RTN28AO2 are the same as for RTN28O2 in original CRI v2.2 R5 except for accretion product formation. RTN28AO2 does not undergo autoxidation.

42. $RTN28AO2 + NO = 0.23RTN28NO3 + 0.77TNCARB26 + 0.77NO2 : 2.7D-12 * EXP(360/TEMP) * 0.767 ;$

43. $RTN28AO2 + HO2 = RTN28OOH : 2.91D-13 * EXP(1300/TEMP) * 0.914 ;$

295 44. $RTN28AO2 + NO3 = TNCARB26 + HO2 + NO2 : 2.3D-12 ;$

45. $RTN28AO2 = TNCARB26 : 6.65E-13 * RO2 ;$

46. $RTN28AO2 = 0.5 C20d : 0.4E-11 * RO2_b ;$

47. $RTN28AO2 = 0.667C15d : 1.8E-12 * RO2_m ;$

Reactions of RTN28BO2

300 Reaction with HO2 forms hydroperoxide species already in CRI, not a HOM due to insufficient oxygens.

48. $RTN28BO2 + HO2 = RTN28OOH : KRO2HO2 * 0.914 ;$

Reaction with NO, NO3 forms next generation OHRO2 via alkoxy radical isomerisation and fragmentation products (smaller RO2, RN9O2, and closed shell species, CARB16) at 50:50 branching ratio). NO also forms small yield of RN18NO3, estimated from original CRI v2.2 R5.

305 49. $RTN28BO2 + NO = 0.125 * RTN28NO3 + 0.875CH3COCH3 + 0.875RN19O2 + 0.875NO2 : KRO2NO ;$

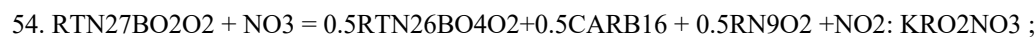
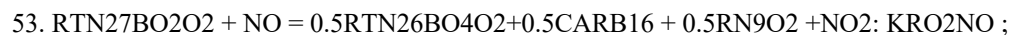
50. $RTN28BO2 + NO3 = CH3COCH3 + RN17O2 + NO2 : KRO2NO3 ;$

Autoxidation of RTN28BO2 to produce 2nd generation OHRO2, RTN27BO2O2

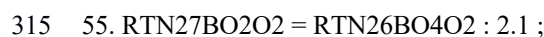
51. $RTN28BO2 = RTN27BO2O2 : 2.1 ;$

Reactions of RTN27BO2O2

310 Reaction with HO2 forms hydroperoxide species already in CRI, not a HOM due to insufficient oxygens.

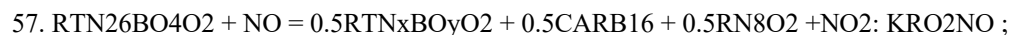
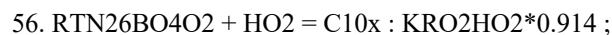


Autoxidation of RTN27BO2O2 to produce 3rd generation OHRO2, RTN26BO4O2

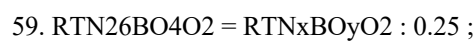


Reactions of RTN26BO4O2

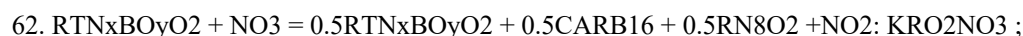
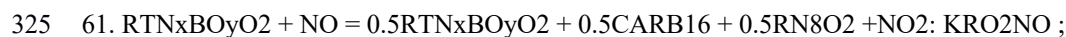
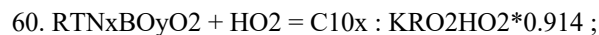
Hydroperoxide from RTN26BO4O2 has sufficient oxygens to be classified as a HOM.



Autoxidation of RTN26BO4O2 to produce “4th generation and higher” OHRO2, RTNxBOyO2

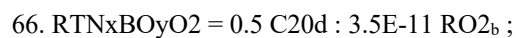
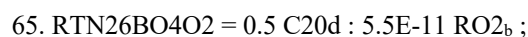
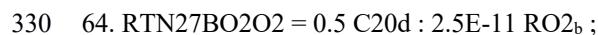


Reactions of RTNxBOyO2 - no further autoxidation occurs



Reactions of OHRO2 with big peroxy radical pool (RO2_b)

Rate coefficient from fitting of model to experimental data (Berndt et al, 2018b).



Reactions of OHRO2 with medium, small and total peroxy radical pools (RO2_m, RO2_s and RO2)



335 68. $RTN27BO2O2 = 0.4TNCARB26 + 0.3RTN26BO4O2 + 0.3CARB16 + 0.3RN10O2 : 5E-12*RO2 ;$

69. $RTN26BO4O2 = 0.4C10x + 0.3RTNxBOyO2 + 0.3CARB16 + 0.3RN9O2 : 8E-12*RO2 ;$

70. $RTNxBOyO2 = 0.8C10x + 0.1RTNxBOyO2 + 0.1CARB16 + 0.1RN8O2 : 1E-11*RO2 ;$

Rate coefficient of OHRO2 with isoprene-derived peroxy radical from fitting of model to experimental data (Berndt et al, 2018b).

340 71. $RTN28BO2 = 0.667C15d : 1.8E-12 RO2_m ;$

72. $RTN27BO2O2 = 0.667C15d : 3.75E-12 RO2_m ;$

73. $RTN26BO4O2 = 0.667C15d : 3.75E-12 RO2_m ;$

74. $RTNxBOyO2 = 0.667C15d : 3.75E-12 RO2_m ;$

Photolysis of HOMs

345 Photolysis of peroxide linkage and carbonyl linkages were considered using MCM frequencies J41 and J22 respectively. The KPP parameter “SUN” was used in experiments where the photolysis frequency was varied.

Photolysis of peroxide linkage in HOM monomer produces one OH and one alkoxy radical which behaves as previously discussed (50% decomposition, 50% isomerisation). As the extent of oxidation of the HOM is unknown, isomerisation produces second generation peroxy radical by default.

350 75. $C10z = 0.5CARB16 + 0.5RN9O2 + 0.5RN25BO2O2 + OH : J41;$

76. $C10x = 0.5CARB16 + 0.5RN9O2 + 0.5RTN27BO2O2 + OH : J41;$

Photolysis of C20d produces two alkoxy radicals. The isomerisation products are 2nd gen OHRO2 and 2nd gen O3RO2.

77. $C20d = 0.5RN25BO2O2 + 0.5RTN27BO2O2 + RN9O2 + CARB16 : J41;$

355 Photolysis of C15d produces two alkoxy radicals. The isoprene-derived alkoxy radical produces UCARB12 (as inCRI v2.2 R5) while the alkoxy radical from alpha pinene forms next generation peroxy radicals via isomerisation (50 % OHRO2 and 50% O3RO2) and fragmentation products.

78. $C15d = UCARB12 + 0.25RN25BO2O2 + 0.25RTN27BO2O2 + 0.5RN9O2 + 0.5CARB16 : J41;$

Photolysis of carbonyl linkage produces an acyl radical and an alkyl radical which will form peroxy radicals. It is assumed that one of these peroxy radicals is big enough to be considered (2nd generation) O3RO2 or OHRO2

360 79. $C10z = RN25BO2O2 : J22;$

80. $C10x = RTN27BO2O2 : J22;$

81. $C20d = RN25BO2O2 + RTN27BO2O2 : J22;$

For C15d, one of the two peroxy radicals formed is assumed to be of medium size and produce UCARB12 which isomerisation (as occurs for isoprene-derived peroxy radicals).

365 82. C15d = 0.5RN25BO2O2 + 0.5RTN27BO2O2 + UCARB12: J22;

HOM loss to OH

All HOM species are lost to OH with same rate coefficient as that for large hydroperoxide RTN28OOH in CRI v2.2 R5. The products, closed shell CRI species CARB10 and CARB15, were chosen under the assumption that the HOM fragments and the sum of CRI indices of the product is close to the CRI index of the peroxy radical which formed the HOM (23-27). The
370 reaction of C15d also produces a product featured in the oxidation pathway of isoprene, UCARB10.

83. C10z + OH = CARB10 + CARB15 + OH : 2.38E-11 ;

84. C10x + OH = CARB10 + CARB15 + OH : 2.38E-11 ;

85. C15d + OH = CARB10 + CARB15 + UCARB10+ OH : 2.38E-11 ;

86. C20d + OH = 2CARB10 + 2CARB15 + OH : 2.38E-11 ;

375

Table S5 - Temperature dependencies used for 3 temperature dependent mechanism versions.

Species	HOM ₆₀₀₀	HOM ₉₀₀₀	HOM ₁₂₀₇₇
RN26BO2	1.223E8*EXP(-6000/T)	2.981E12*EXP(-9000/T)	9.413E16*EXP(-12077/T)
RN25BO2O2	1.009E9*EXP(-6000/T)	2.460E13*EXP(-9000/T)	7.768E17*EXP(-12077/T)
RN24BO4O2	1.009E9*EXP(-6000/T)	2.460E13*EXP(-9000/T)	7.768 E17*EXP(-12077/T)
RN23BO6O2	9.500E8*EXP(-6000/T)	2.315E13*EXP(-9000/T)	7.311E17*EXP(-12077/T)
RTN28BO2	1.247E9*EXP(-6000/T)	3.038E13*EXP(-9000/T)	9.595E17*EXP(-12077/T)
RTN27BO2O2	1.247E9*EXP(-6000/T)	3.038E13*EXP(-9000/T)	9.595E17*EXP(-12077/T)
RTN26BO4O2	1.484E8*EXP(-6000/T)	3.617E12*EXP(-9000/T)	1.142E17*EXP(-12077/T)

The uncertainty in the autoxidation coefficients was estimated by further box models simulations where an autoxidation coefficient was adjusted so that the corresponding species was simulated at the upper and lower concentrations values given
380 the experimental uncertainty.

Table S6 – References for model parameters and confidence

Parameter	Value(s)	Source	Confidence
-----------	----------	--------	------------

Autoxidation Coefficients	Detailed in Table 4	Derived in this work*	Estimated uncertainty in Table 4
Rate coefficients for C20d formation (k13)	Section 2.3.1 and SI reaction list: 21, 23, 25, 27, 29, 46, 63, 64, 65, 66	Derived in this work	Sensitivity tests suggested uncertainty range of +100% / - 35% (scalings of 0.65-2)
Rate coefficients for C15d formation (k16)	Section 2.3.2 and SI reaction list: 36, 37, 38, 39, 40, 47, 71, 72, 73, 74	Derived in this work	Sensitivity tests suggested uncertainty range of $\pm 50\%$ (scalings of 0.5-1.5)
Closed Shell / Alkoxy radical from a specific big RO ₂ reacting with RO ₂ b pool (k14, k15)	Section 2.3.1 and SI reaction list: 22, 24, 26, 28, 30, 32-35	Molteni et al (2019), Roldin et al (2019)	Scaling by factors of 10 and 0.1 did not affect rate coefficients fitted for autoxidation or accretion product formation. HOM yield greater sensitivity with universal scalings of +100% and -50% resulting in a doubling and halving of HOM yield respectively.
k14/k15 branching ratio	50:50	Ratio similar to Jenkin et al (2019a) values of 40:60 (1°, 2° RO ₂), 20:80 (3° RO ₂)	Sensitivity tests with ratios of 40:60 and 20:80 did not affect rate coefficients fitted for autoxidation or accretion product formation and had minor effects on HOM yield.
HOM + OH rate coefficient	2.38×10^{-11} molecules ⁻¹ cm ³ s ⁻¹	Based on comparable species in CRI v2.2, RTN28OOH	Increasing rate coefficient to collision limit (as suggested by Bianchi et al., 2019) had negligible affect
Alkoxy radical decomposition-isomerisation branching ratio	50:50	Estimate	<u>Sensitivity tests with ratios of 75:25 and 25:75 did not affect rate coefficients fitted for autoxidation or accretion product formation.</u> HOM yield below 200 ppt NO _x was unaffected and at 2 ppb NO _x , uncertainty in autoxidation temperature dependence dwarfed this uncertainty. Ratio more important at higher NO _x but this coincided with drastically reduced HOM yield.

*Note that the autoxidation rate coefficient for the 1st generation species RTN28BO2 was taken from Xu et al (2018)

385

Breakdown of Peroxy Radical Pools In CRI-HOM

Large Peroxy Radical Pool (8 or more carbons)

RTN28AO2, RTN28BO2, RTN27BO2O2, RTN26BO4O2, RTNxBOyO2, RN26BO2, RTN24O2, RN25BO2O2,
RN24BO4O2, RN23BO6O2, RNxBOnO2, NRTN28O2, RA19CO2, RTX28O2, NRTX28O2, RTN26O2, RTN25O2,
390 RTX22O2, RTN24O2, RTN23O2

Medium Peroxy Radical Pool (4-7 carbons)

RU12O2, NRU12O2, RN13O2, RN12O2, NRN12O2, RA13O2, DHPR12O2, RN11O2, RA16O2, RU10O2, RU10AO2,
MACO3, RN13AO2, RU12O2, NRU12O2, RTN14O2, RN16AO2, RN14O2, RTN10O2, RN17O2, RN15AO2, RN15O2,
RN18AO2, RN16O2, RN18O2, RN19O2

395 Small Peroxy Radical Pool (3 or fewer carbons)

CH3O2, C2H5O2, HOCH2CH2O2, CH3CO3, C2H5CO3, ICH3H7O2, RN10O2, HOCH2CO3, NRN6O2, RN9O2, NRN9O2,
RN8O2

References

Bates, K. H. and Jacob, D. J.: A new model mechanism for atmospheric oxidation of isoprene: global effects on oxidants,
400 nitrogen oxides, organic products, and secondary organic aerosol, Atmos. Chem. Phys., 19, 9613–9640, doi.org/10.5194/acp-
19-9613-2019, 2019.

Berndt, T., Mentler, B., Scholz, W., Fischer, L., Herrmann, H., Kulmala, M. and Hansel, A.: Accretion product formation from
ozonolysis and OH radical reaction of α -pinene: mechanistic insight and the influence of isoprene and ethylene. Environmental
405 science & technology, 52,11069-11077, doi.org/10.1021/acs.est.8b02210, 2018b.

Jenkin, M. E., Valorso, R., Aumont, B., and Rickard, A. R.: Estimation of rate coefficients and branching ratios for reactions
of organic peroxy radicals for use in automated mechanism construction, Atmos. Chem. Phys., 19, 7691–7717,
doi.org/10.5194/acp-19-7691-2019, 2019a.

410

Lee, S.H., Uin, J., Guenther, A.B., de Gouw, J.A., Yu, F., Nadykto, A.B., Herb, J., Ng, N.L., Koss, A., Brune, W.H. and
Baumann, K.: Isoprene suppression of new particle formation: Potential mechanisms and implications. Journal of Geophysical
Research: Atmospheres, 121,14-621, doi.org/10.1002/2016JD024844, 2016.

415 Molteni, U., Simon, M., Heinritzi, M., Hoyle, C.R., Bernhammer, A.K., Bianchi, F., Breitenlechner, M., Brilke, S., Dias, A.,
Duplissy, J. and Frege, C.: Formation of Highly Oxygenated Organic Molecules from α -Pinene Ozonolysis: Chemical
Characteristics, Mechanism, and Kinetic Model Development. ACS Earth and Space Chemistry, 3, 873-
883,doi.org/10.1021/acsearthspacechem.9b00035, 2019.

420 Rinne, H.J.I., Guenther, A.B., Greenberg, J.P. and Harley, P.C.: Isoprene and monoterpene fluxes measured above Amazonian
rainforest and their dependence on light and temperature. Atmos Env, 36, 2421-2426. doi.org/10.1016/S1352-2310(01)00523-
4, 2002

Roldin, P., Ehn, M., Kurtén, T., Olenius, T., Rissanen, M.P., Sarnela, N., Elm, J., Rantala, P., Hao, L., Hyttinen, N. and
425 Heikkinen, L.: The role of highly oxygenated organic molecules in the Boreal aerosol-cloud-climate system. Nature
communications, 10, 1-15, doi.org/10.1038/s41467-019-12338-8, 2019.

Scott, C. E., Rap, A., Spracklen, D. V., Forster, P. M., Carslaw, K. S., Mann, G. W., Pringle, K. J., Kivekäs, N., Kulmala, M., Lihavainen, H., and Tunved, P.: The direct and indirect radiative effects of biogenic secondary organic aerosol, *Atmos. Chem. Phys.*, 14, 447–470, doi.org/10.5194/acp-14-447-2014, 2014.

Sihto, S.-L., Kulmala, M., Kerminen, V.-M., Dal Maso, M., Petäjä, T., Riipinen, I., Korhonen, H., Arnold, F., Janson, R., Boy, M., Laaksonen, A., and Lehtinen, K. E. J.: Atmospheric sulphuric acid and aerosol formation: implications from atmospheric measurements for nucleation and early growth mechanisms, *Atmos. Chem. Phys.*, 6, 4079–4091, doi:10.5194/acp-6-4079-2006, 2006.

Xu, L., Møller, K.H., Crounse, J.D., Otkjær, R.V., Kjaergaard, H.G. and Wennberg, P.O.: Unimolecular reactions of peroxy radicals formed in the oxidation of α -pinene and β -pinene by hydroxyl radicals. *The Journal of Physical Chemistry A*, 123, 1661-1674, doi.org/10.1021/acs.jpca.8b11726, 2019.